Finite-Difference Time-Domain Simulation of Ground Penetrating Radar on Dispersive, Inhomogeneous, and Conductive Soils

F. L. Teixeira, Weng Cho Chew, *Fellow, IEEE*, M. Straka, M. L. Oristaglio, *Member, IEEE*, and T. Wang

***Abstract*— A three-dimensional (3-D) time-domain numerical scheme for simulation of ground penetrating radar (GPR) on dispersive and inhomogeneous soils with conductive loss is described. The finite-difference time-domain (FDTD) method is used to discretize the partial differential equations for time stepping of the electromagnetic fields. The soil dispersion is modeled by multiterm Lorentz and/or Debye models and incorporated into the FDTD scheme by using the piecewise-linear recursive convolution (PLRC) technique. The dispersive soil parameters are obtained by fitting the model to reported experimental data. The perfectly matched layer (PML) is extended to match dispersive media and used as an absorbing boundary condition to simulate an open space. Examples are given to verify the numerical solution and demonstrate its applications. The 3-D PML-PLRC-FDTD formulation facilitates the parallelization of the code. A version of the code is written for a 32-processor system, and an almost linear speedup is observed.**

***Index Terms*—Absorbing boundary conditions, dispersive media, electromagnetic underground propagation, finite-difference time-domain (FDTD) methods.**

I. Introduction

LINEAR dispersive media are often encountered in nature, such as in rocks, soils, ice, snow, or plasma [1]–[7]. In rocks and soils, dispersive phenomena can result from dielectric relaxation in the media. This could be, for instance, a consequence of the geometrical effect of insulating rock platelets immersed in a conductive host [6]. Moreover, it could be the result of the interaction of electromagnetic fields with the double layer around colloidal suspensions in a saline solution [7]. When the permittivity varies as a function of frequencies, the conductivity varies as a function of frequencies, as dictated by the causality requirement of the Kramers–Kronig relations [8].

Manuscript received May 27, 1997; revised November 21, 1997. This work was supported by the Air Force Office of Scientific Research under MURI Grant F49620-96-1-0025, Office of Naval Research under Grant N00014-95-1-0872, National Science Foundation under Grant ECS93-02145, and a CAPES Graduate Fellowship.

F. L. Teixeira and W. C. Chew are with the Center for Computational Electromagnetics, Department of Electrical and Computer Engineering, University of Illinois, Urbana, IL 61801-2991 USA (e-mail: w-chew@uiuc.edu).

M. Straka is with the National Center for Supercomputing Applications, University of Illinois, Urbana, IL 61801-2991 USA.

M. L. Oristaglio is with the Electromagnetics Department, Schlumberger–Doll Research, Ridgefield, CT 06877 USA.

T. Wang is with Western Atlas Logging Services, Houston, TX 77252 USA.

Publisher Item Identifier S 0196-2892(98)05635-6.

At the operating frequency range (50–1000 MHz) of ground penetrating radar (GPR), soil materials can exhibit strongly dispersive properties. For example, experimental data [1] show that effective permittivity and effective conductivity of wet soils can vary over 20% and by factors greater than two at frequencies of 30 and 500 MHz, respectively. In such media, broadband electromagnetic waves will propagate and attenuate in a frequency-dependent manner. Therefore, to have a realistic model of propagation of electromagnetic waves on the lossy earth, it is prudent to include the effect of dispersion in the media. Understanding of these effects is useful for the correct interpretation of radargrams. For the model, either a Lorentz relaxation model or a Debye relaxation model will be assumed [9]–[11]. Both are causal models, so that the Kramers–Kronig relations are automatically satisfied. Because of this, the permittivity value will be complex, having both a frequency-dependent real and imaginary part. The imaginary part can be thought of as frequency-dependent loss or conductivity in addition to the static conductivity. Throughout this paper, the term dispersion will refer to dispersion in the sense of a Lorentz–Debye model (i.e., finite relaxation times), although, rigorously speaking, any media with static conductivity (infinite relaxation time) is already dispersive (in the sense of having a frequency-dependent response).

The amount of interest devoted to time-domain numerical methods to solve electromagnetic problems have been increasing dramatically in recent years. This is due partly to its conceptual simplicity and great flexibility to treat practical problems. Along with the continuous progress of the available computational resources, two recent algorithmic developments in the finite-difference time-domain (FDTD) method make even more attractive the direct numerical simulation of the time-domain electromagnetic field propagation in complex, dispersive media in open space.

The first one is the family of techniques developed to incorporate dispersion effects into existing FDTD schemes, which can be roughly characterized into three types:

1) z-transform method [4];
2) auxiliary differential equation (ADE) method [12]–[14];
3) recursive convolution (RC) technique [9], [10], [15], [16].

The former two are usually more accurate, while the latter is usually more efficient in terms of CPU time and storage requirements. In addition, the RC technique provides easier

treatment for the case of dispersive media with multiple poles in the susceptibility function, an important aspect for treatment of more complex media. A recently proposed extension of the RC technique [and demonstrated for one-dimensional (1-D) problems] is the piecewise-linear recursive convolution (PLRC) [17], which has an accuracy similar to the other approaches and retains the advantages of the RC approach. In this paper, we apply the PLRC technique to a three-dimensional (3-D) simulation. Since the PLRC is a *local* modification on the update equations, there is no conceptual difference between the PLRC as applied to 1-D simulations and the PLRC for two-dimensional (2-D) and 3-D simulations.

The second recent development in the FDTD method consisted in the introduction of the perfectly matched layer (PML) as an absorbing boundary condition (ABC) [18]–[20] to simulate open space on a finite computational grid. Apart from its numerical efficiency, one of the major advantages of the PML over the previously proposed ABC [21]–[24] is that its absorption properties hold independently of the frequency of the incident wave. Also, most previously proposed ABC's are not suited for dispersive media because they require knowledge of the wave velocity near the grid boundary, a quantity that is not well defined in the time domain for dispersive media. Another advantage of the PML is that it preserves the nearest-neighbor-interaction characteristic of the FDTD method, making it ideally suited for implementation on a single-instruction multiple-data (SIMD) massively parallel computer.

However, the PML, as originally devised, also applies only to nondispersive media. In order to apply it for GPR simulations in dispersive media, it is necessary to extend the PML to handle dispersive media. Very recently, the first extensions of the PML to dispersive media for a 1-D PML (single planar boundary) were considered in [25] and [26]. The extension proposed in [25] was based on the anisotropic PML formulation [27]. A single-term Lorentz media was considered. The dispersive modeling was implemented using the ADE approach, making it difficult to extend for media with multiterm dispersion models. On the other hand, the extension in [26] was based on a modification of the original PML approach of Berenger [18], and, as a result, a different set of frequency-dependent constitutive parameters had to be carefully derived for the PML media to achieve the perfect matching condition for the dispersive media at all frequencies. Moreover, this extension is dependent on the specific choice of dispersion model being used (i.e., Lorentz, Drude, Debye, etc.). Also, in [25] and [26], no indication is given on how to treat, using these approaches, the PML corner regions of the computational domain, which play a pivotal role in 2-D and 3-D simulations.

In contrast, this paper extends the PML to 3-D dispersive media by using the complex coordinate stretching approach [20]. Some advantages of using this approach for dispersive media can be listed as follows.

1) There is no need to derive constitutive parameters for the PML medium. This is because, to achieve the perfect matching condition in this approach, the *same* constitutive parameters can be assumed *everywhere* (i.e., both in the physical and PML regions). The PML region is then simply defined as the region where the complex stretching is enforced.
2) Treatment of corner regions poses no special difficulty since it just corresponds to regions where simultaneous stretching in different directions are enforced. Therefore, 2-D and 3-D simulations can be easily treated. To illustrate this point, all of the equations in the formulation will be presented for a situation in which there are simultaneous stretching on all three directions. Cases with stretching only along some of the coordinates are just special cases of the equations presented with the complex stretching variables on the remaining coordinates set equal to unity.
3) It is particularly suited to be combined with the dispersion modeling techniques based on recursive convolution, such as the PLRC, thus providing easier treatment of multiterm Lorentz or Debye models.
4) Since the same set of equations is used both inside the physical and PML regions (the physical region can be considered as a special case of a PML region with all complex stretching variables equal to unity), an easier parallelization of the code is made possible.

Some previous numerical simulations of GPR using the FDTD method or the closely related transmission-line matrix (TLM) method were considered in [28]–[38]. In particular, the recent 3-D analysis of [35] already included dispersion effects and a detailed modeling of the receiving and transmitting antennas. However, no ABC was used to truncate the computational domain, so that unwanted reflections due to the grid termination were presented and had to be eliminated through windowing the results in time (which required larger simulation domains) combined with a subtracting procedure (which required multiple simulations). Also, the dispersion model used was a simplified one in the sense that a low-frequency approximation was used for the single-term Debye model.

In this paper, the extension of the 3-D PML to dispersive media outlined above is combined with the PLRC technique in a unified numerical scheme to further enhance the accuracy of FDTD simulations of electromagnetic wave propagation for GPR applications. Multiterm second-order Lorentz and first-order Debye dispersion models for the soils are explicitly treated in this scheme. In the time-domain, the resultant 3-D PML-PLRC-FDTD scheme is implemented based on a split form of Maxwell's equations. The dispersive soils model parameters are obtained by curve-fitting reported experimental data. Examples including the response of buried objects on dispersive soils with conductive loss are given to verify the numerical solutions and demonstrate its applications. To illustrate the suitability of the proposed numerical scheme to parallel simulations, a parallelized version of the code is written for a 32-processor system and is shown to have an almost linear speedup.

II. PML-FDTD Formulation of Dispersive Media

The PML ABC can be related to a complex coordinate stretching in the frequency domain [20]. This complex stretch-

ing modifies the Maxwell's equations by adding additional degrees of freedom to achieve the reflectionless absorption of the waves inside the PML region. In the time-domain, the electromagnetic fields components need to be split into subcomponents. This splitting generally doubles the memory requirements of an FDTD simulation. When conductive loss is added, this further increases the memory requirements because of an added conductivity term in the PML equation. It will be shown that the inclusion of dispersion further increases the memory requirements.

The modified Maxwell's equations in the complex coordinate stretching PML formulation are [20]

$$\nabla_s \times \mathbf{E} = i\omega \mathbf{B} \tag{1}$$

$$\nabla_s \times \mathbf{H} = -i\omega \mathbf{D} + \sigma \mathbf{E} \tag{2}$$

for a conductive medium and in the frequency domain ($e^{-i\omega t}$ convention). In the above

$$\nabla_s = \hat{x}\,\frac{1}{s_x}\,\partial_x + \hat{y}\,\frac{1}{s_y}\,\partial_y + \hat{z}\,\frac{1}{s_z}\,\partial_z \tag{3}$$

where s_x, s_y, and s_z are frequency-dependent complex stretching variables. To facilitate the solution in the time domain, (1) and (2) are usually split as follows:

$$i\omega \mathbf{B}_{sx} = \frac{1}{s_x}\,\partial_x \hat{x} \times \mathbf{E} \tag{4}$$

$$-i\omega \mathbf{D}_{sx} + \sigma \mathbf{E}_{sx} = \frac{1}{s_x}\,\partial_x \hat{x} \times \mathbf{H} \tag{5}$$

where the same is repeated for y and z replacing x.

By letting $s_x = a_x + i(\Omega_x/\omega)$, where a_x and Ω_x are frequency independent, the above becomes

$$i\omega a_x \mathbf{B}_{sx} - \Omega_x \mathbf{B}_{sx} = \partial_x \hat{x} \times \mathbf{E} \tag{6}$$

$$-i\omega a_x \mathbf{D}_{sx} + \Omega_x \mathbf{D}_{sx} + a_x \sigma \mathbf{E}_{sx} + i\,\frac{\Omega_x}{\omega}\,\sigma \mathbf{E}_{sx} = \partial_x \hat{x} \times \mathbf{H}. \tag{7}$$

The variables Ω_x and a_x are the added degrees of freedom of the modified Maxwell's equations. The variable $\Omega_x \geq 0$ induces the reflectionless absorption of propagating modes inside the PML, and the variable $a_x \geq 1$ enhances the attenuation rate of evanescent waves, if they exist. In the physical domain, $\Omega_x = 0$ and $a_x = 1$, so that the above equations reduce to the usual Maxwell's equations. Transforming the above back into the time domain, we obtain

$$-a_x \partial_t \mathbf{B}_{sx} - \Omega_x \mathbf{B}_{sx} = \partial_x \hat{x} \times \mathbf{E} \tag{8}$$

$$a_x \partial_t \mathbf{D}_{sx} + \Omega_x \mathbf{D}_{sx} + a_x \sigma \mathbf{E}_{sx} + \Omega_x \sigma \int_0^t \mathbf{E}_{sx}(\tau)\,d\tau = \partial_x \hat{x} \times \mathbf{H}. \tag{9}$$

In the above, for a dispersive medium, we let $\mathbf{B}_{sx} = \mu \mathbf{H}_{sx}$ while

$$\mathbf{D}_{sx}(t) = \epsilon(t) * \mathbf{E}_{sx}(t). \tag{10}$$

An N-species Lorentzian dispersive medium is characterized by a frequency-dependent relative permittivity function given by

$$\epsilon(\omega) = \epsilon_0[\epsilon_\infty + \chi(\omega)] = \epsilon_0\epsilon_\infty + \epsilon_0(\epsilon_s - \epsilon_\infty) \sum_{p=1}^{N} \frac{G_p \omega_p^2}{\omega_p^2 - i2\omega\alpha_p - \omega^2} \tag{11}$$

where $\chi(\omega)$ is the medium susceptibility, ω_p is the resonant frequency for the pth species, α_p is the correspondent damping factor, and ϵ_0, ϵ_∞ are the static and infinite frequency permittivities, respectively. In the time domain, a complex susceptibility function [10] can be defined

$$\hat{\chi}(t) = \sum_{p=1}^{P} \hat{\chi}_p(t) = \sum_{p=1}^{P} i\gamma_p e^{(-\alpha_p - i\beta_p)t} u(t) \tag{12}$$

where

$$\beta_p = \sqrt{\omega_p^2 - \alpha_p^2} \tag{13a}$$

$$\gamma_p = \frac{\omega_p^2 G_p(\epsilon_s - \epsilon_\infty)}{\sqrt{\omega_p^2 - \alpha_p^2}} \tag{13b}$$

and

$$\sum_{p=1}^{P} G_p = 1 \tag{13c}$$

so that the time-domain susceptibility function is $\mathcal{F}^{-1}[\chi(\omega)] = \chi(t) = \Re e[\hat{\chi}(t)]$ and $\epsilon(t) = \epsilon_0[\epsilon_\infty \delta(t) + \chi(t)]$. For a Debye model, the frequency-dependent permittivity function is written as

$$\epsilon(\omega) = \epsilon_0[\epsilon_\infty + \chi(\omega)] = \epsilon_0\epsilon_\infty + \epsilon_0 \sum_{p=1}^{N} \frac{A_p}{1 - i\omega\tau_p}. \tag{14}$$

In this formula, A_p is the pole amplitude and τ_p is the relaxation time for the pth species. Note that the complex susceptibility function for the Debye relaxation model can be considered as a special case of (12) when $\alpha_p > \omega_p$ and $\Im m(\beta_p) < 0$. Hence, the expression (12) applies to *both* models through a proper choice of parameters.

The electric flux is related to the electric field via

$$\mathbf{D}(t) = \epsilon_0\epsilon_\infty \mathbf{E}(t) + \epsilon_0 \chi(t) * \mathbf{E}(t). \tag{15}$$

Using (12) in (15), we have, for both models

$$\mathbf{D}(t) = \epsilon_0\epsilon_\infty \mathbf{E}(t) + \epsilon_0 \sum_{p=1}^{P} \Re e[\hat{\chi}_p(t) * \mathbf{E}(t)]. \tag{16}$$

When $t = l\Delta_t$ and using a piecewise-linear approximation for the electric field in the time-discretization scheme, such that

$$\mathbf{E}(t) = \mathbf{E}^l + \frac{(t - l\Delta_t)}{\Delta_t}\,(\mathbf{E}^{l+1} - \mathbf{E}^l) \tag{17}$$

(16) then becomes

$$\mathbf{D}^l = \epsilon_0\epsilon_\infty \mathbf{E}^l + \epsilon_0 \sum_{p=1}^{P} \Re e[\mathbf{Q}_p^l] \tag{18}$$

where

$$\mathbf{Q}_p^l = \sum_{m=0}^{l-1} \left[(\hat{\chi}_p^0 - \hat{\zeta}_p^0)\mathbf{E}^{l-m} + \hat{\zeta}_p^0 \mathbf{E}^{l-m-1} \right] e^{-(\alpha_p + i\beta_p)m\Delta_t}. \tag{19}$$

In the above, $\hat{\chi}_p^0$ and $\hat{\zeta}_p^0$ are constants, which depend on the parameters of the particular model, given by

$$\begin{aligned} \hat{\chi}_p^0 &= \int_0^{\Delta_t} \hat{\chi}_p(t)\, dt \\ &= \frac{i\gamma_p}{\alpha_p + i\beta_p} \left[1 - e^{-(\alpha_p + i\beta_p)\Delta_t} \right] \qquad (20a) \\ \hat{\zeta}_p^0 &= \int_0^{\Delta_t} t\hat{\chi}_p(t)\, dt \\ &= \frac{i\gamma_p}{\Delta_t(\alpha_p + i\beta_p)^2} \{ 1 - [(\alpha_p + i\beta_p)\Delta_t + 1] \\ &\qquad \times e^{-(\alpha_p + i\beta_p)\Delta_t} \}. \qquad (20b) \end{aligned}$$

$\mathbf{Q}_p^l$ can be calculated recursively through

$$\mathbf{Q}_p^l = \begin{cases} 0, & l = 0 \\ (\hat{\chi}_p^0 - \hat{\zeta}_p^0)\mathbf{E}^l + \hat{\zeta}_p^0 \mathbf{E}^{l-1} + \mathbf{Q}_p^{l-1} e^{-i\tilde{\omega}_p \Delta_t}, & l > 0 \end{cases} \tag{21}$$

where $\tilde{\omega}_p = \beta_p - i\alpha_p$.

The above equations allow the computation of $\mathbf{D}^l$ given $\mathbf{E}^l$ as the input. However, we would like to compute $\mathbf{E}^l$ given $\mathbf{D}^l$ as the input in an FDTD scheme, as we shall see later. To this end, we substitute (21) into (18) to obtain

$$\begin{aligned} \mathbf{D}^l = {} & \epsilon_0 \left(\epsilon_\infty + \sum_{p=1}^{P} \Re e\left[\hat{\chi}_p^0 - \hat{\zeta}_p^0 \right] \right) \mathbf{E}^l + \epsilon_0 \sum_{p=1}^{P} \Re e[\hat{\zeta}_p^0] \mathbf{E}^{l-1} \\ & + \epsilon_0 \sum_{p=1}^{P} \Re e\left[\mathbf{Q}_p^{l-1} e^{-i\tilde{\omega}_p \Delta_t} \right] \end{aligned} \tag{22}$$

or that

$$\mathbf{D}^l = \epsilon_0 (\lambda_0 \mathbf{E}^l + \lambda_1 \mathbf{E}^{l-1} + \mathbf{P}^{l-1}) \tag{23}$$

where

$$\lambda_0 = \epsilon_\infty + \sum_{p=1}^{P} \Re e\left[\hat{\chi}_p^0 - \hat{\zeta}_p^0 \right] \tag{24a}$$

$$\lambda_1 = \sum_{p=1}^{P} \Re e\left[\hat{\zeta}_p^0 \right] \tag{24b}$$

$$\mathbf{P}^{l-1} = \sum_{p=1}^{P} \Re e\left(\mathbf{Q}_p^{l-1} e^{-i\tilde{\omega}_p \Delta_t} \right) \tag{24c}$$

depends only on $\mathbf{Q}_p^{l-1}$.

III. Time-Stepping Scheme

We need to devise a time-stepping scheme for (8) and (9). The space discretization is done according to the usual Yee staggered-grid with central differencing scheme [39] so that we will not discuss it here. The time discretization for them is as follows:

$$\begin{aligned} & \frac{-a_x(\mathbf{B}_{sx}^{l+(1/2)} - \mathbf{B}_{sx}^{l-(1/2)})}{\Delta_t} - \Omega_x \mathbf{B}_{sx}^{l+(1/2)} \\ & \quad = \partial_x \hat{x} \times \mathbf{E}^l, \qquad (25) \\ & \frac{a_x(\mathbf{D}_{sx}^{l+1} - \mathbf{D}_{sx}^{l})}{\Delta_t} + \Omega_x \mathbf{D}_{sx}^{l+1} + a_x \sigma \mathbf{E}_{sx}^{l+1} + \sigma \Omega_x \mathbf{F}_{sx}^{l} \\ & \quad = \partial_x \hat{x} \times \mathbf{H}^{l+(1/2)} \qquad (26) \end{aligned}$$

where $\mathbf{F}(t) = \int_0^t \mathbf{E}(\tau)\, d\tau$. Equation (25) can be easily rearranged for time stepping

$$\begin{aligned} & \mathbf{B}_{sx}^{l+(1/2)} \\ & \quad = -(a_x + \Omega_x \Delta_t)^{-1} \left[\Delta_t (\partial_x \hat{x} \times \mathbf{E}^l) - a_x \mathbf{B}_{sx}^{l-(1/2)} \right] \qquad (27) \\ & (a_x + \Omega_x \Delta_t)\mathbf{D}_{sx}^{l+1} + a_x \sigma \Delta_t \mathbf{E}_{sx}^{l+1} \\ & \quad = \Delta_t (\partial_x \hat{x} \times \mathbf{H}^{l+(1/2)}) + a_x \mathbf{D}_{sx}^{l} - \sigma \Omega_x \Delta_t \mathbf{F}_{sx}^{l}. \qquad (28) \end{aligned}$$

However, the left-hand side of (28) depends on both $\mathbf{D}_{sx}^{l+1}$ and $\mathbf{E}_{sx}^{l+1}$, making it unsuitable for time stepping. To remove this problem, we substitute (23) into the left-hand side of (28) so that we have

$$\begin{aligned} & [(a_x + \Omega_x \Delta_t)\lambda_0 \epsilon_0 + a_x \sigma \Delta_t] \mathbf{E}_{sx}^{l+1} \\ & \quad = \Delta_t (\partial_x \hat{x} \times \mathbf{H}^{l+(1/2)}) + a_x \mathbf{D}_{sx}^{l} - \sigma \Omega_x \Delta_t \mathbf{F}_{sx}^{l} \\ & \qquad - (a_x + \Omega_x \Delta_t)\epsilon_0 (\lambda_1 \mathbf{E}_{sx}^{l} + \mathbf{P}_{sx}^{l}). \end{aligned} \tag{29}$$

The above equation is now suitable for time stepping and updating $\mathbf{E}_{sx}^{l+1}$. After $\mathbf{B}_{sx}^{l+(1/2)}$ is updated and hence $\mathbf{H}_{sx}^{l+(1/2)}$ is updated, it is used in (29) to update $\mathbf{E}_{sx}^{l+1}$. On the right-hand side of (29), the other pertinent quantities are updated as follows:

$$\mathbf{D}_{sx}^{l} = \epsilon_0 \left(\lambda_0 \mathbf{E}_{sx}^{l} + \lambda_1 \mathbf{E}_{sx}^{l-1} + \mathbf{P}_{sx}^{l-1} \right) \tag{30a}$$

$$\mathbf{F}_{sx}^{l} = \mathbf{F}_{sx}^{l-1} + \tfrac{1}{2} \left(\mathbf{E}_{sx}^{l} + \mathbf{E}_{sx}^{l-1} \right) \Delta_t \tag{30b}$$

$$\mathbf{Q}_{p,\,sx}^{l} = (\hat{\chi}_p^0 - \hat{\zeta}_p^0)\mathbf{E}_{sx}^{l} + \hat{\zeta}_p^0 \mathbf{E}_{sx}^{l-1} + \mathbf{Q}_{p,\,sx}^{l-1} e^{-i\tilde{\omega}_p \Delta_t} \tag{30c}$$

$$\mathbf{P}_{sx}^{l} = \sum_{p=1}^{P} \Re e\left[\mathbf{Q}_{p,\,sx}^{l} e^{-i\tilde{\omega}_p \Delta_t} \right]. \tag{30d}$$

The above scheme is repeated for x replaced with y and z. Hence, (27), (29), and (30) constitute the complete PML-PLRC-FDTD updating scheme for the electromagnetic fields. Note that, due to the use of a backward Euler's method (forward difference in time) in the time-update scheme of (25) and (26) and the neglect of $\mathbf{F}^{l+1}$ in (26) [which differs from $\mathbf{F}^l$ by $O(\Delta_t)$], the above scheme is only first-order accurate in time. This is chosen mainly due to its simplicity and to the fact that less arithmetic operations are required at each time step. Another advantage is that this is a conditionally stable scheme in the diffusion regime. If needed, a second-order accurate scheme can be easily derived through parallel lines, by employing, for example, a trapezoidal rule time-update scheme (leapfrog scheme). However, this last scheme, when combined with the central-differencing scheme in space characteristic of the FDTD method, is not stable anymore in the diffusion regime [8].

Storage is required for $\mathbf{H}_{s\xi}$, $\mathbf{E}_{s\xi}$, $\mathbf{F}_{s\xi}$, $\mathbf{Q}_{p,s\xi}$, $p=1,\cdots,P$, $\xi=x,y,z$, and since each $\mathbf{A}_{s\xi}$ has two vector components, we need to store $(18+6P)N$ values where N is the number of simulation nodes and P is the number of species in the relaxation model. The added storage cost of simulating a PML dispersive medium is $6PN$, while the added cost of a PML conductive medium is to store $\mathbf{F}_{s\xi}$, which is $6N$. A nondispersive, nonconductive PML medium will require $12N$ storage as opposed to the $6N$ needed in the plain Yee scheme. Although (29) and (30) seem to suggest the need to store the electric field at two successive time steps, this can be avoided in the numerical algorithm by storing, at each time step, the electric field at the previous time step in a temporary variable [17]. Therefore, the use of a piecewise-linear approximation (17) in the constitutive relation $\mathbf{D}(t)=\epsilon(t)*\mathbf{E}(t)$ does not incur additional storage requirements in comparison to a piecewise-constant approximation. It should be pointed out that arbitrary susceptibility functions can, in principle, be modeled as a sum of Lorentz and/or Debye terms. This can be done, e.g., by first evaluating the dielectric permittivity and the effective conductivity for various frequencies and then curve fitting the result by a meromorphic function expanded as a partial fraction expansion [40] with (possibly) single poles (Debye terms), complex conjugate poles (Lorentz terms), and a pole at $\omega_p=0$ (static conductivity term), plus a constant term standing for the permittivity at infinite frequency. This will be illustrated in the next section.

IV. Numerical Simulation Results

An FDTD code has been written using the formulation of previous sections. A PML medium is assumed everywhere so that the code can be easily parallelized, allowing operation in the SIMD (single-instruction multiple-data) mode.

To first validate the formulation, the results from the FDTD simulation for a homogeneous dispersive half-space problem with conductive loss are compared against a pseudoanalytical solution. The pseudoanalytical solution is obtained by first numerically integrating the frequency-domain Sommerfeld integrals of the half-space problem for many excitation frequencies [8]. The result is then multiplied by the spectrum of the source pulse and, subsequently, inverse Fourier transformed to yield the time-domain solution. Fig. 1 compares the results for the FDTD simulation using both the PML-RC (piecewise-constant electric field) approach and the PML-PLRC (piecewise-linear electric field) in a dispersive half-space against this pseudo-analytical solution. The half-space dispersion parameters are obtained by fitting a two-species ($P=2$) Debye model [33] to the experimental data reported by Hipp [1] for the Puerto Rico type of claim loams, as given in Table I. The experimental and model data are plotted in Figs. 2 and 3. As seen, the model data fit the experimental data reasonably well. The specific curve taken for the comparison of Fig. 1 is the 5% moisture content case with the model parameters given in Table I. The PML for this example is set with ten layers with a quadratic taper [18]–[20]. The source pulse is the first derivative of a slightly different version of the Blackmann–Harris pulse [41] so that the pulse vanishes completely after a time period $T=1.55/f_c$. The central frequency is at $f_c=200$ MHz. Note that with this frequency of operation (typical of GPR applications) and with the relaxation times presented in Table I, we have $\omega_c\tau_p>1$, so that it is not possible to use a low-frequency approximation for the Debye model. The half-space occupies 60% of the vertical height of the cubic simulation region. The simulation is done with a $N_x\times N_y\times N_z=50\times 50\times 50$ grid with

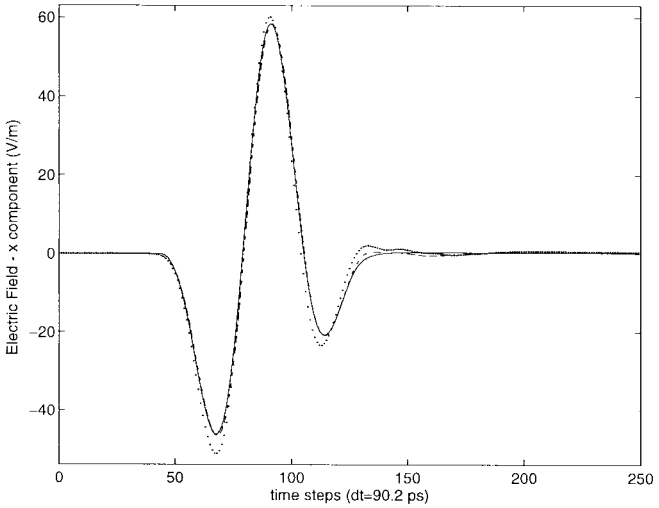

Fig. 1. Sommerfeld solution (solid line) versus PML-FDTD solution using RC (dotted line) and PLRC (dashed line) for an infinitesimal vertical electric dipole radiating on top of a dispersive half-space modeled by a two-species Debye model. The PLRC approach presents a better agreement against the pseudoanalytical Sommerfeld solution.

TABLE I
Debye-Model Parameters of the Puerto Rico-Type Clay Loams

moisture	ϵ_∞	σ(mS/m)	A_1	A_2	τ_1(nsec)	τ_2(nsec)
2.5%	3.20	.397	0.75	0.30	2.71	0.108
5%	4.15	1.11	1.80	0.60	3.79	0.151
10%	6.00	2.00	2.75	0.75	3.98	0.251

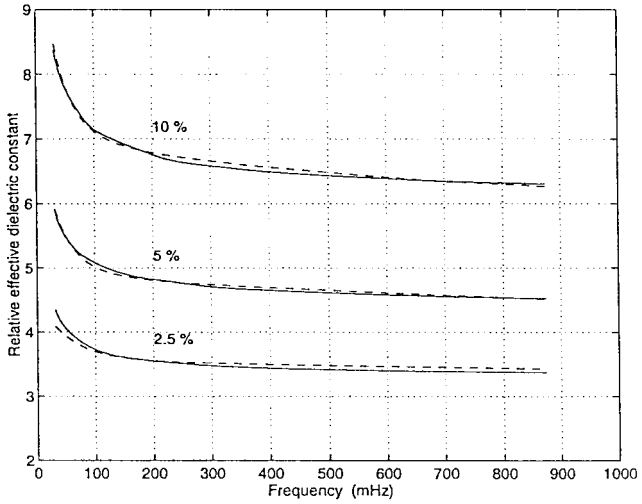

Fig. 2. Dielectric permittivity of the Puerto Rico type of clay loams versus frequency [1]. The solid lines indicate the experimental data, and the dashed lines indicate the model-fitting data. The numbers indicate the content of moisture.

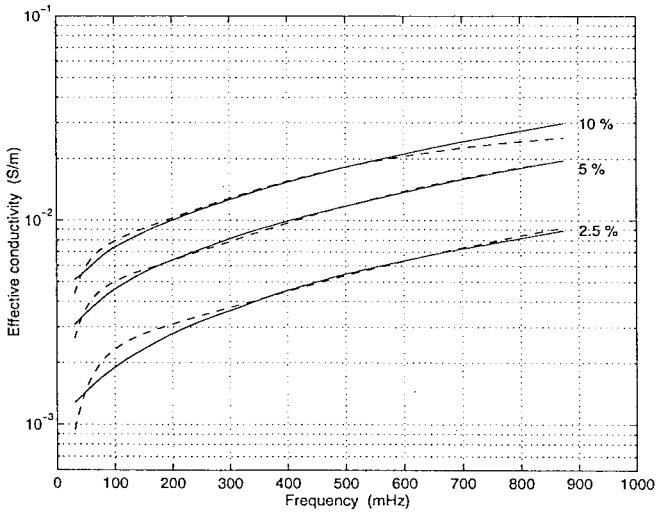

Fig. 3. Same as Fig. 2, except for the effective conductivity.

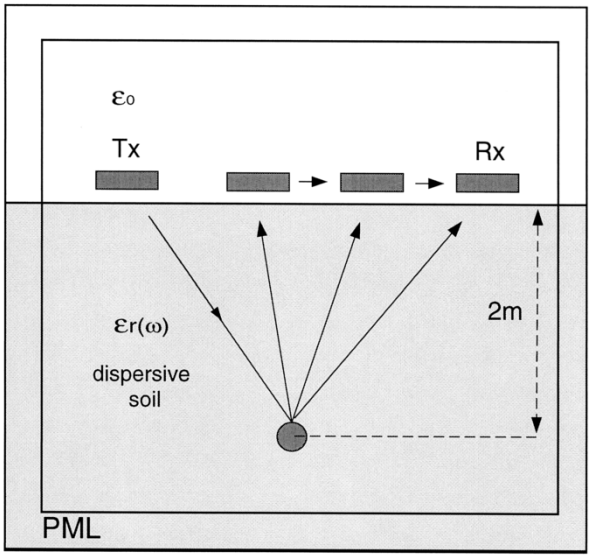

Fig. 4. Common-source configuration of the GPR. See text for details.

a space discretization size $\Delta_s = 5.86$ cm and a time step $\Delta_t = 90.2$ ps. Assuming that the origin is at a corner of the cube, the source is a vertical electric dipole (y-directed) located at $(x, y, z) = (25, 35, 25)\Delta_s$ and the x-component of the electric field is sampled at $(x, y, z) = (15, 25, 25)\Delta_s$. The field is deliberately sampled inside the half-space so that it is more sensitive to its dispersive properties.

The results show an agreement between the formulations. In particular, this figure illustrates the improvement in accuracy by using the PLRC against the RC scheme. Also, no noticeable reflection due to the grid termination is present.

In what follows, a series of examples of the numerical simulation of the GPR response of a pipeline buried on the Puerto Rico type of claim loams with different moisture contents will be presented. The pipe is either metallic or plastic, buried 2 m deep, and has a diameter of 6 in. Both the transmitter and receiver dipoles are parallel to the metal pipe. Note that this is a $2.5D$ problem [30]; i.e., there is invariance of the geometry in one direction (meaning the inhomogeneity is 2-D), but the field distribution is 3-D due to the source configuration. In this kind of problems, we can take advantage of the *spatial* invariance in one dimension and apply a Fourier transformation in that direction to eliminate one of the spatial derivatives in Maxwell's equations. This allows a properly modified 2-D FDTD scheme to solve the full-wave 3-D problem [30], [33]. In our simulations, however, it will be solved using the full 3-D code. The simulation is done with a $N_x \times N_y \times N_z = 80 \times 70 \times 40$ grid. The space discretization is $\Delta_s = 0.05$ m, and the time step is $\Delta_t = 77.0$ ps. The air–ground interface is located at $y = 55\Delta_s$. The pipe points in the z direction and is centered at $(x, y) = (35, 15)\Delta_s$. The transmitter and receiver are located just above the ground. The transmitter is fixed at $(x, y, z) = (15, 57, 25)\Delta_s$, and the receiver moves in a straight line in the z direction (perpendicular to the pipe), from the point $(x, y, z) = (17, 57, 25)\Delta_s$ to the point $(x, y, z) = (65, 57, 25)\Delta_s$ so that the source-receiver offset varies from 0.1 to 2.5 m. Fig. 4 illustrates this common-source configuration. Since the emphasis is on the wave propagation modeling aspect, both the transmitter and receiver considered are just point electric dipoles. For an example on a direct incorporation of a more realistic antenna modeling using the FDTD scheme, refer to the approaches described in [34] and [35], where bowtie antennas are considered. Alternatively, we can also incorporate aperture antennas directly in the model by using an array of equivalent point dipoles positioned on the antenna aperture, with the strength parameters (weights) of each dipole being determined by a calibration procedure [38].

For these examples, the source pulse used is again a derivative of the Blackmann–Harris pulse centered at 200 MHz. The PML absorbing boundary condition is set with ten PML with a quadratic taper increasing from the physical domain interface toward the grid ends.

Fig. 5(a)–(c) compare the numerical simulation, with and without dispersion included, of the common-source radar traces for a metal pipe ($\sigma = 10^6$) in soils with 2.5, 5, and 10% of moisture. The model parameters for the simulation with dispersion are taken from Table I, and the constitutive parameters of the simulation without dispersion are taken from Figs. 2 and 3 at the center frequency of 200 MHz. The simulated traces are normalized to the maximum field value at the receiver for each receiver position. From Fig. 5 (a)–(c), we first note that, for increased moisture content, the simulated echo appears later and is subjected to a stronger attenuation, in agreement with Figs. 2 and 3, where it is seen that both the effective conductivity and the effective dielectric constant increases with increasing moisture contents.

To better illustrate the effects of the dispersion on the reflected pulse, Fig. 6(a)–(c) single out a view of the simulated traces obtained with the simulation with and without dispersion [same cases of Fig. 5(a)–(c)] at a specific offset of 2.0 m. Despite the insignificant differences on the first arrival times, it is seen that the dispersion may distort the pulse shape against the nondispersive simulation. For example, in Fig. 6(a), the reflected pulse in the presence of dispersion becomes less symmetric with respect to its main lobe than in the simulation without dispersion.

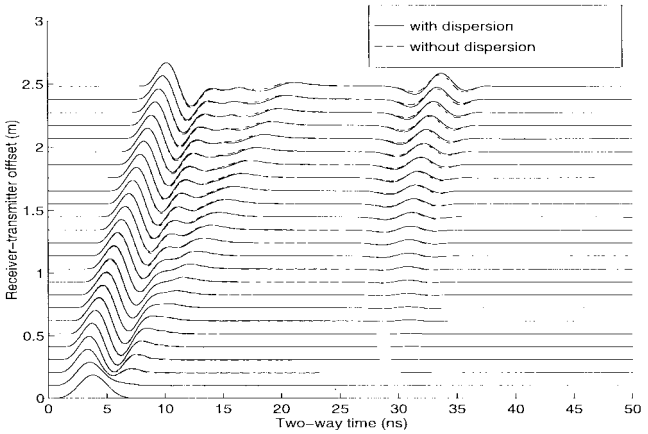

(a)

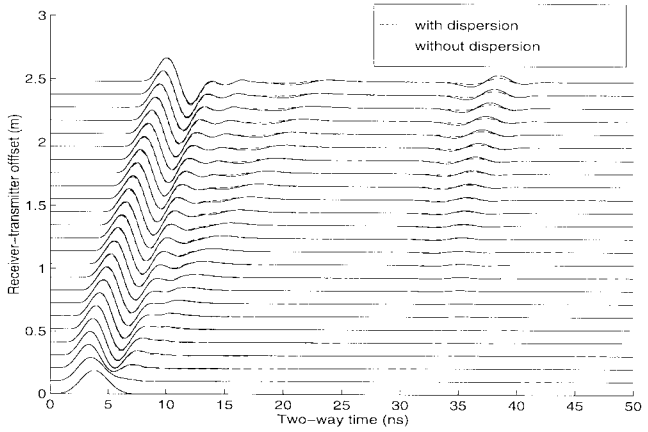

(b)

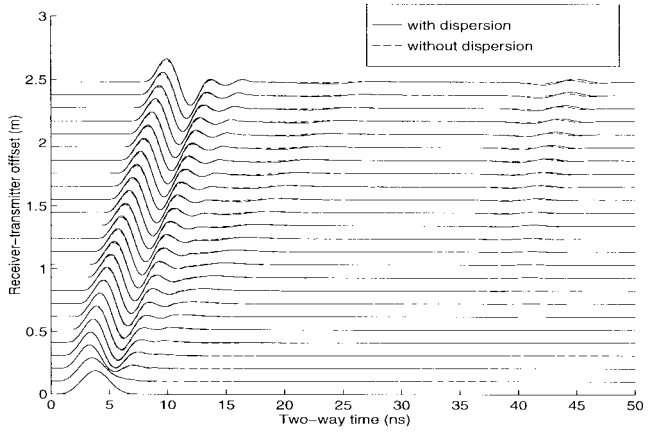

(c)

Fig. 5. Simulation of the radar traces (common-source configuration), calculated with and without dispersion, of a metal pipe on a soil with: (a) 2.5%, (b) 5.0%, and (c) 10.0% of moisture. The dielectric constant and conductivity for the simulation without dispersion are picked from Figs. 2 and 3 at the central frequency of 200 MHz. Increased moisture contents tend to slow and increase the attenuation of the reflected pulse from the pipe.

Fig. 7 presents the simulated radar traces of a plastic pipe $(\epsilon_r = 2, \sigma = 0)$ on a soil with 2.5% of moisture, with dispersion modeling included and model parameters taken from Table I, against a simulation without dispersion with constitutive parameters taken from Figs. 2 and 3 at 200 MHz.

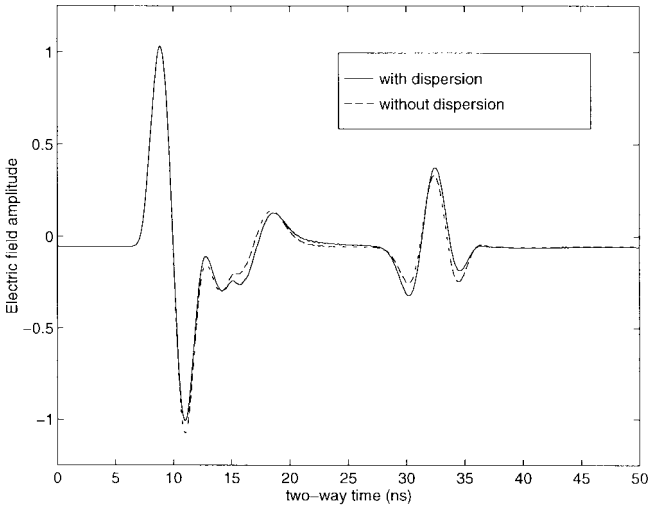

(a)

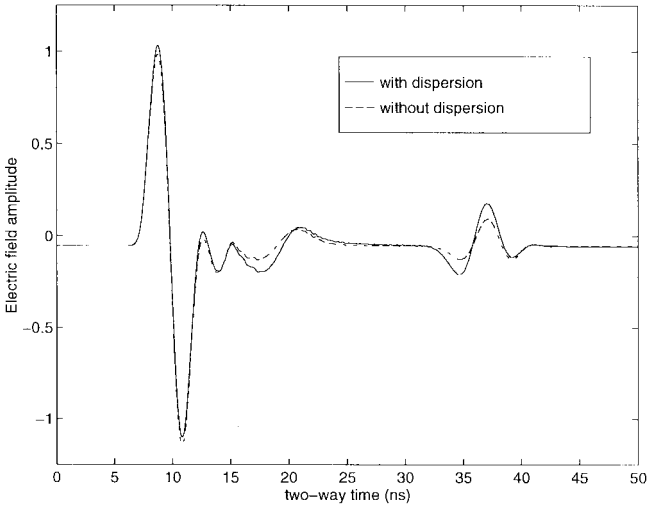

(b)

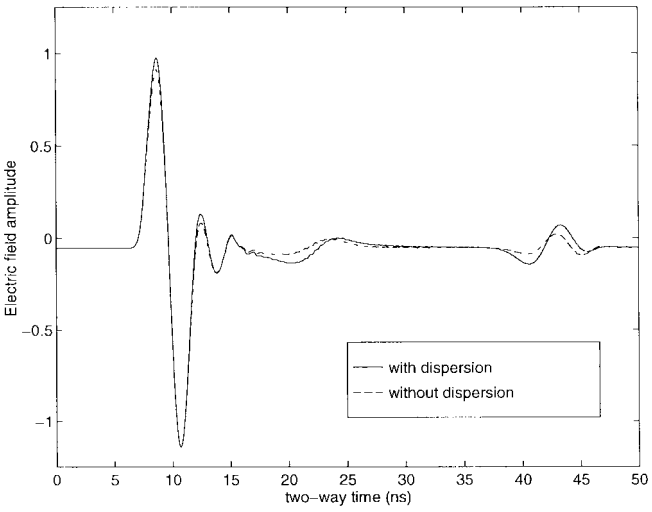

(c)

Fig. 6. Radar trace simulation taken from Fig. 5(a)–(c) at an offset of 2.0 m, calculated with and without dispersion, in soils with: (a) 2.5%, (b) 5.0%, and (c) 10.0% of moisture.

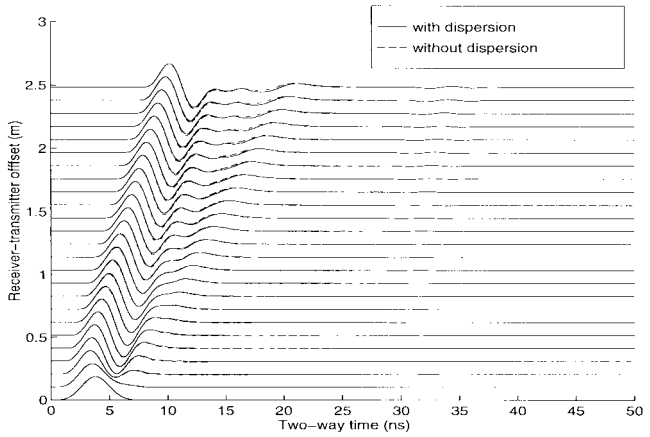

Fig. 7. Simulation of the radar trace (common-source configuration), calculated with and without dispersion, of a plastic pipe on a soil with 2.5% of moisture. The dielectric constant and conductivity for the simulation without dispersion are picked from Figs. 2 and 3 at the central frequency of 200 MHz. Due to the less-reflective nature of the plastic material, the reflected trace is less visible.

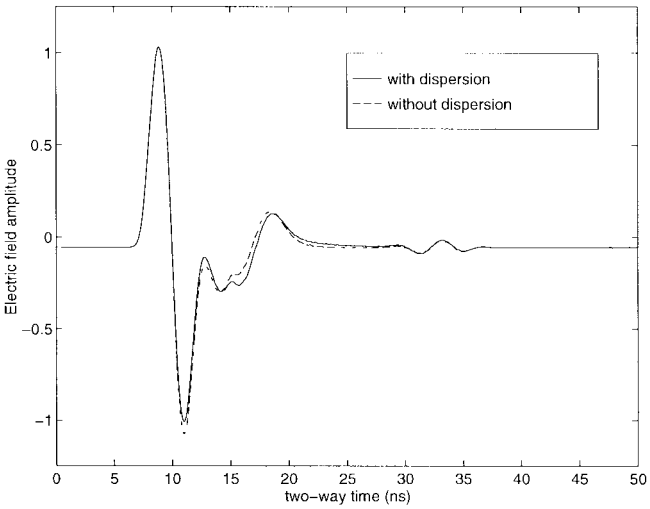

Fig. 8. Radar trace simulation taken from Fig. 7 at an offset of 2.0 m, calculated with and without dispersion.

The geometry is the same as in the metallic pipe example. Due to the less-reflective nature of the plastic material, the reflected trace is now much weaker.

Fig. 8 singles out the simulated response of the plastic pipe response taken at an offset of 2 m for the dispersive and nondispersive cases. The difference between the reflected pulses for the dispersive and nondispersive cases is less apparent than in the metallic case.

It should be emphasized that the above observations are made based on the specific choice of the nondispersive soil parameters and on the kind of soil and buried object considered. The details may vary for different choices of the parameters and soils. It is not the intention here to exhaust these scenarios.

A version of the code has been parallelized to run on a 32-processor SGI R10000. Fig. 9 shows the speed of the code (running a two-species dispersive model) for 1000 time steps as a function of the number of active processors. The speed

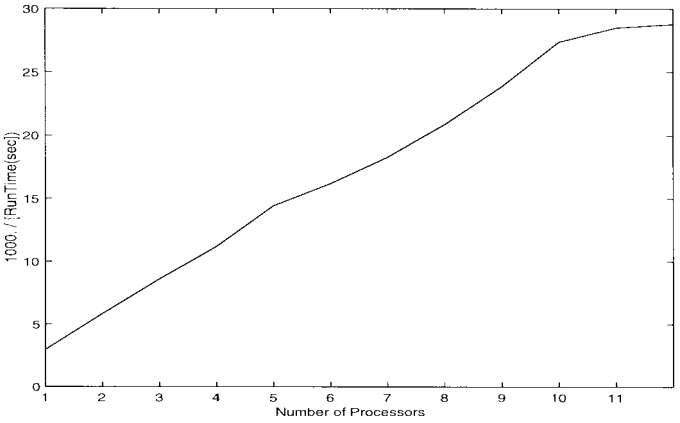

Fig. 9. Speed of the code as a function of the number of processors on a 32-processor SGI R10000 machine. The problem size is $50 \times 50 \times 50$. An almost linear speedup is observed up to 12 active processors, but performance deteriorates for this problem size as the number of processors further increases.

is defined as the inverse of the real CPU time on an empty machine (single-user). The problem size is $50 \times 50 \times 50$. An almost linear speedup to 12 processors is observed. For this problem size, not much more speedup past 12–15 processors is expected due to the communication overhead and load imbalance between the processors. However, for larger problems sizes, increased speedup can be expected with a larger number of active processors.

V. Conclusions

A 3-D FDTD numerical simulation of the GPR response on dispersive media with conductive loss is described. The dispersive effect is modeled by a multiterm Lorentz and/or Debye model. The electric field convolution is implemented by the PLRC. The PML is extended to match dispersive media and used as an absorbing boundary condition. By a proper choice of the parameters, the media can exhibit the dispersive effects observed in some soils and rocks. The 3-D PML-PLRC-FDTD numerical simulations with buried metal and plastic pipes buried on dispersive soils show that the reflected pulse (and, hence, the GPR response) can be affected by dispersive effects. In addition to its inherent numerical efficacy, the use of the PML allows the easy parallelization of the code. However, the use of the PML and dispersive media modeling comes with the added cost of more memory requirements and computational time. A version of the code was paralleled and shown to have an almost linear speedup.

Acknowledgment

The authors acknowledge the reviewers for their useful suggestions regarding this paper. Part of the computer time was provided by the National Center for Supercomputing Applications, University of Illinois.

References

[1] J. E. Hipp, "Soil electromagnetic parameters as functions of frequency, soil density, and soil moisture," *Proc. IEEE*, vol. 62, pp. 98–103, Jan. 1974.

[2] W. D. Hurt, "Multiterm Debye dispersion relations for permittivity of muscle," *IEEE Trans. Biomed. Eng.*, vol. 32, pp. 60–64, Jan. 1985.
[3] D. Sullivan, "A frequency-dependent FDTD method for biological applications," *IEEE Trans. Microwave Theory Tech.*, vol. 40, pp. 532–539, Apr. 1992.
[4] ———, "Frequency-dependent FDTD methods using z transforms," *IEEE Trans. Antennas Propagat.*, vol. 40, pp. 1223–1230, Nov. 1992.
[5] O. P. Gandhi, B. Q. Gao, and J. Y. Chen, "A frequency-dependent finite-difference time-domain formulation for general dispersive media," *IEEE Trans. Microwave Theory Tech.*, vol. 41, pp. 658–664, May 1993.
[6] P. N. Sen and W. C. Chew, "The frequency dependent dielectric and conductivity response of sedimentary rocks," *J. Microw. Power*, vol. 18, no. 1, p. 95, 1983.
[7] W. C. Chew and P. N. Sen, "Dielectric enhancement due to electrochemical double layer: Thin double layer approximation," *J. Chem. Phys.*, vol. 77, no. 9, p. 4683, 1982.
[8] W. C. Chew, *Waves and Fields in Inhomogeneous Media.* New York: Van Nostrand Reinhold, 1990, reprinted by IEEE Press, 1995, ch. 4.
[9] R. Luebbers, F. P. Hunsgerger, K. S. Katz, R. B. Standler, and M. Schneider, "A frequency-dependent finite-difference time-domain formulation for dispersive materials," *IEEE Trans. Electromagn. Compat.*, vol. 32, pp. 222–227, Feb. 1990.
[10] R. Luebbers and F. P. Hunsberger, "FDTD for N-th order dispersive media," *IEEE Trans. Antennas Propagat.*, vol. 40, pp. 1297–1301, Dec. 1992.
[11] C. M. Rappaport and W. H. Weedon, "Computational issues in ground penetrating radar," Center Electromagn. Res., Northeastern Univ., Boston, MA, Unpublished Rep., 1994.
[12] T. Kashiva, Y. Ohtomo, and I. Fukai, "A finite-difference time-domain formulation for transient propagation in dispersive media associated with Cole–Cole's circular arc law," *Microwave. Opt. Technol. Lett.*, vol. 3, no. 12, pp. 416–419, 1990.
[13] R. M. Joseph, S. C. Hagness, and A. Taflove, "Direct time integration of Maxwell's equations in linear dispersive media with absorption for scattering and propagation of femtosecond electromagnetic pulses," *Opt. Lett.*, vol. 16, pp. 1412–1414, 1991.
[14] O. P. Gandhi, B.-Q. Gao, and J.-Y. Chen, "A frequency-dependent finite-difference time-domain formulation for general dispersive media," *IEEE Trans. Microwave Theory Tech.*, vol. 41, pp. 658–664, May 1993.
[15] M. D. Bui, S. S. Stuchly, and G. I. Coustache, "Propagation of transients in dispersive dielectric media," *IEEE Trans. Microwave Theory Tech.*, vol. 39, pp. 1165–1171, Oct. 1991.
[16] R. J. Hawkins and J. S. Kallman, "Linear electronic dispersion and finite-difference time-domain calculations: A simple approach," *J. Lightwave Technol.*, vol. 11, pp. 1872–1874, 1993.
[17] D. F. Kelley and R. J. Luebbers, "Piecewise linear recursive convolution for dispersive media using FDTD," *IEEE Trans. Antennas Propagat.*, vol. 44, pp. 792–797, June 1996.
[18] J. P. Berenger, "A perfectly matched layer for the absorption of electromagnetic waves," *J. Comput. Phys.*, vol. 114, pp. 185–200, 1994.
[19] D. S. Katz, E. T. Thiele, and A. Taflove, "Validation and extension to three dimensions of the Berenger PML absorbing boundary condition for FD-TD meshes," *IEEE Microwave Guided Wave Lett.*, vol. 4, pp. 268–270, Feb. 1994.
[20] W. C. Chew and W. H. Weedon, "A 3D perfectly matched medium from modified Maxwell's equations with stretched coordinates," *Microwave Opt. Technol. Lett.*, vol. 7, pp. 599–604, 1994.
[21] A. Bayliss and E. Turkel, "Radiation boundary conditions for wave-like equations," *Commun. Pure Appl. Math.*, vol. 33, pp. 707–725, 1980.
[22] G. Mur, "Absorbing boundary conditions for the finite-difference approximation of the time domain electromagnetic field equations," *IEEE Trans. Electromagn. Compat.*, vol. EMC-23, pp. 377–382, May 1981.
[23] Z. P. Liao, H. L. Wong, B. P. Yang, and Y. F. Yuan, "A transmitting boundary for transient wave analysis," *Scientia Sinica-A*, vol. 27-A, pp. 1063–1076, 1984.
[24] K. K. Mei and J. Fang, "Superabsorption—A method to improve absorbing boundary conditions," *IEEE Trans. Antennas Propagat.*, vol. 40, pp. 1001–1010, Sept. 1992.
[25] S. D. Gedney, "An anisotropic PML absorbing media for the FDTD simulation of fields in lossy and dispersive media," *Electromagnetics*, vol. 16, pp. 399–415, 1996.
[26] T. Uno, Y. He, and S. Adachi, "Perfectly matched layer absorbing boundary condition for dispersive medium," *IEEE Microwave Guided Wave Lett.*, vol. 7, pp. 264–266, Sept. 1997.
[27] Z. S. Sacks, D. M. Kingsland, R. Lee, and J.-F. Lee, "A perfectly matched anisotropic absorber for use as an absorbing boundary condition," *IEEE Trans. Antennas Propagat.*, vol. 43, pp. 1460–1463, Dec. 1995.
[28] C. Liu and L. C. Chen, "Numerical simulation of subsurface radar for detecting buried pipes," *IEEE Trans. Geosci. Remote Sensing*, vol. 29, pp. 795–798, July 1991.
[29] M. Moghaddam, W. C. Chew, B. Anderson, E. Yannakis, and Q. H. Liu, "Computation of transient electromagnetic waves in inhomogeneous media," *Radio Sci.*, vol. 26., no. 1, pp. 265–273, 1991.
[30] M. Moghaddam, E. J. Yannakakis, W. C. Chew, and C. Randall, "Modeling of the subsurface interface radar," *J. Electromagn. Waves Applicat.*, vol. 5, pp. 17–39, 1991.
[31] Y. He, T. Uno, S. Adachi, and T. Mashiko, "Two-dimensional active imaging of conducting objects buried on a dielectric half-space," *IEICE Trans. Commun.*, vol. E76-B, no. 12, pp. 1546–1551, 1993.
[32] K. Demarest, R. Plumb, and Z. Huang, "The performance of FDTD absorbing boundary conditions for buried scatterers," in *Proc. URSI Radio Sci. Mtg.*, 1994, p. 169.
[33] T. Wang, M. L. Oristaglio, and W. C. Chew, "Finite-difference simulation of ground penetrating radar in dispersive soils," Schlumberger–Doll Research, Ridgefield, CT, SDR-EMG Res. Note, Dec. 1995.
[34] B. J. Hook, "FDTD modeling of ground-penetrating radar antennas," in *Proc. 11th Annu. Rev. Prog. Appl. Comp. Electromag.*, Monterey, CA, 1995, pp. 740–747.
[35] J. M. Bourgeois and G. S. Smith, "A fully three-dimensional simulation of a ground-penetrating radar: FDTD theory compared with experiment," *IEEE Trans. Geosci. Remote Sensing*, vol. 34, pp. 36–44, Jan. 1996.
[36] J. Calhoun, "A finite difference time domain (FDTD) simulation of electromagnetic wave propagation and scattering in a partially conducting layered earth," in *Proc. 1997 IGARSS—Int. Geosci. Remote Sensing Symp.*, pp. 922–924.
[37] G. A. Newman and D. L. Alumbaugh, "3D Electromagnetic modeling using staggered finite differences," in *Proc. 1997 IGARSS—Int. Geosci. Remote Sensing Symp.*, pp. 929–931.
[38] S. Agosti, G. G. Gentili, and U. Spagnolini, "Electromagnetic inversion of monostatic GPR: Application to pavement profiling," in *Proc. 1997 Int. Conf. Electromag. Adv. Applicat. (ICEAA'97)*, pp. 491–494.
[39] K. S. Yee, "Numerical solution of initial boundary value problems involving Maxwell's equation in isotropic media," *IEEE Trans. Antennas Propagat.*, vol. 14, pp. 302–307, Feb. 1966.
[40] E. C. Levy, "Complex-curve fitting," *IRE Trans. Automat. Control*, pp. 37–43, May 1959.
[41] F. J. Harris, "On the use of windows for harmonic analysis with the discrete Fourier transform," *Proc. IEEE*, vol. 66, pp. 51–83, Jan. 1978.

F. L. Teixeira received the M.S.E.E. degree from the Pontifical Catholic University, Rio de Janeiro, Brazil, in 1995. He is currently pursuing the Ph.D. degree in electrical engineering at the University of Illinois at Urbana-Champaign.

He was a Technical Officer with the Brazilian Army Research and Development Center (IPD-CTEx) from 1992 to 1994, and from 1994 to 1996, he was a member of the Technical Staff in the Satellite Transmission Department, EMBRATEL S.A. (Brazilian Telecom). Since 1996, he has been a Research Assistant with the Center for Computational Electromagnetics, University of Illinois at Urbana-Champaign. His research interests include wave propagation modeling for communication and sensing applications.

Weng Cho Chew (S'79–M'80–SM'86–F'93), for a photograph and biography, see p. 748 of the May 1998 issue of this TRANSACTIONS.

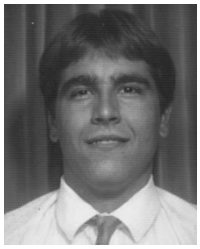

M. Straka received the B.S. degree in computer science and engineering with a minor in astrophysics from the University of Illinois at Urbana-Champaign in 1987.

He has been a Consultant and Applications Programmer with the National Center for Supercomputing Applications (NCSA), University of Illinois at Urbana-Champaign, since 1987. His focus is on performance analysis and optimization techniques for large, scalable scientific applications on vector supercomputers and parallel RISC superscalar processor.

M. L. Oristaglio (M'89) received the B.S. and M.S. degrees in geology and geophysics from Yale University, New Haven, CT, in 1974, and the M.Sc. degree in geochemistry and the D.Phil. degree in geophysics, both from Oxford University, Oxford, U.K., in 1975 and 1978, respectively.

He was a Postdoctoral Research Associate at the University of Utah, Salt Lake City, and a Gibbs Instructor in Geology and Geophysics at Yale University. He is currently Director of Electromagnetics at Schlumberger–Doll Research, Ridgefield, CT, since 1990. He joined Schlumberger in 1982 as a Research Scientist in the Mechanics-Electrical Department. From 1985 to 1987, he was Technical Advisor at Schlumberger Engineering Center, Paris, France. From 1988 to 1990, he was Manager of the Workstation Products Department at Schlumberger Austin System Center, Austin, TX. Currently, he is also an Adjunct Professor in the Department of Geology and Geophysics at the University of Utah and a Visiting Professor in the Department of Electrical Engineering, Delft University of Technology, Delft, The Netherlands. His areas of research are forward and inverse problems in acoustics and electromagnetics, chiefly in applied geophysics.

T. Wang received the M.S. degree in geophysics from the Institute of Geophysics, Chinese Academy of Sciences, Beijing, in 1988 and the Ph.D. degree in geophysics from the University of Utah, Salt Lake City, in 1993.

He was a Postdoctoral Fellow at the University of Utah from 1993 to 1994 and a Postdoctoral Fellow at Schlumberger–Doll Research, Ridgefield, CT, from 1994 to 1995. In 1996, he joined Western Atlas Logging Services, Houston, TX. His present research interests include electromagnetic modeling and imaging, signal processing, and borehole geophysics.